Journal of the Physical Society of Japan
Vol. 76, No. 5, May, 2007, 054501

Coexistence of Collisional Drift and Flute Wave Instabilities in Bounded Linear ECR Plasma

Kunihiro KAMATAKI*, Yoshihiko NAGASHIMA[1], Shunjiro SHINOHARA, Yoshinobu KAWAI[1], Masatoshi YAGI[1], Kimitaka ITOH[2], and Sanae-I. ITOH[1]

Interdisciplinary Graduate School of Engineering Sciences, Kyushu University, Kasuga, Fukuoka 816-8580
[1]*Research Institute for Applied Mechanics, Kyushu University, Kasuga, Fukuoka 816-8580*
[2]*National Institute for Fusion Science, Toki, Gifu 509-5292*

(Received November 28, 2006; accepted March 6, 2007; published May 10, 2007)

This paper reports the experimental and theoretical investigation on the coexistence of the collisional drift and flute wave instabilities in the bounded linear electron cyclotron resonance (ECR) plasma. The drift wave instability is excited by the steep density gradient and imposed axial boundary conditions in the device. The flute instability is excited by the bad curvature of the magnetic field. Emphasis is made on the effect of the ion–neutral (i–n) particle collisions. It is observed that the drift wave instability is excited when the i–n particle collision frequency ν_{in} is low, but it is stabilized when ν_{in} is high. Furthermore, the drift and flute modes are coexistent for the intermediate values of ν_{in}. The Hasegawa–Wakatani model which describes the dispersion relation of the collisional drift-interchange mode is used for understanding the experimental observations. It is found that the experimentally observed drift frequency is consistent with the numerical calculation. The present result has shown that the i–n particle collisions play an important role in the stabilization of the collisional drift wave instability in the ECR plasma.

KEYWORDS: collisional drift wave instability, flute wave instability (interchange mode), ion–neutral particle collision frequency, electron cyclotron resonance, turbulence
DOI: 10.1143/JPSJ.76.054501

1. Introduction

The plasma turbulence and its role in anomalous transport are crucial issues in high temperature plasma physics. The nonlinear self-regulation mechanism of drift wave turbulence has been subject to attentions in order to clarify the structural formation of plasma turbulence.[1,2] Recent experimental progress has allowed the direct measurement of the nonlinear coupling in the drift wave turbulence coupled with zonal flows,[3] and yet further detailed studies are necessary. In drift wave turbulence theories,[4–7] the development of turbulence is governed in part by the relative strength of the $\mathbf{E} \times \mathbf{B}$ drift to the ion polarization drift, and in part by the parallel electron dissipation, i.e., plasma adiabaticity. Fluctuations in the range of drift wave frequencies are destabilized by dissipations (such as the collisional drift instability and the dissipative trapped electron instability) or by the reactive instabilities [such as flute instability or ion-temperature-gradient (ITG) mode instability].[2,8] Difference in the evolution of dissipation-driven instabilities and that of reactive instabilities has attracted attentions. For instance, the transition from the ITG mode turbulence to the drift wave instability at a certain critical temperature gradient is one of the key issues in the study of anomalous transport.[1]

The drift wave is well known as a universal low frequency instability driven by the free energy provided by a pressure gradient transverse to the magnetic field.[2] In mirror machines, the averaged magnetic curvature is responsible of an effective gravity, which allows the flute instability to develop. In linear devices with low temperature plasmas (a few eV) it is easier to control the input power and filling gas pressure, and allow us to investigate the competition between the dissipative instability and the reactive instability, i.e., the drift mode and flute mode. The drift wave instability has been extensively studied in linear magnetized plasmas in different plasma parameter regimes,[9] including weakly ionized, fully ionized,[10] collisionless[11] and collision plasmas.[11] Recently, experiments to investigate the structure of low frequency instabilities and turbulence in low temperature plasmas have been performed.[12–25] Light *et al.* observed a low frequency instability identified as a hybrid of the collisional drift wave and the Kelvin–Helmholtz instability in the liner helicon plasma.[15] Brochard *et al.* presented the transition from flute modes to drift modes in a thermionic discharge double plasma.[21] It is well known that the growth rate of collisional drift instability is influenced by the electron–ion collision frequency.[8] However, the ion–neutral particle collisions should be taken into account in weakly ionized plasma as well, and its importance has been shown theoretically.[26] We will show both experimentally and theoretically that it influences the growth rate of the drift wave instability.

In this paper, we investigate the excitation of drift wave instability and flute wave instability using the bounded linear electron cyclotron resonance (ECR) plasma device.[27–29] Emphasis is put on the influence of the ion–neutral particle collisions on the drift and flute (interchange) modes. The flute wave instability has been observed in this device and was reported in the literature.[27] The drift wave instability can be excited by inducing the steep radial gradient and by imposing the axial boundary condition. We find that the drift wave instability occurs when the ion–neutral collision frequency ν_{in} is low, but is stabilized when ν_{in} is high. Furthermore, the drift and flute modes are coexistent for the intermediate values of ν_{in}. Conditions, for which drift and flute waves coexist, are identified. We then study the

*E-mail: kamataki@aees.kyushu-u.ac.jp

dependence of the growth rate and the frequency of collisional drift-interchange (flute) instability on ν_{in} using Hasegawa–Wakatani model. The numerical result explains the experimental dependencies of the growth rate and the frequency on the filling gas pressure.

The paper is organized as follows. In §2 we will describe the experimental apparatus including the diagnostic method. The experimental results of the coexistence of the drift and flute wave instabilities are presented in §3. The set of Hasegawa–Wakatani model equations used in ECR plasma is explained and a comparison between the experimental results and the numerical ones is presented in §4. The discussion and conclusions are given in §5.

2. Experimental Apparatus

The schematic diagram of the ECR plasma device and the axial magnetic field profile are shown in Figs. 1(a) and 1(b), respectively. The cylindrical vacuum chamber consists of stainless steel with the inner diameter (i.d.) is 400 mm and the axial length L is 1200 mm. Argon gas is fed into the vacuum chamber at $z = 300$ mm using a mass flow controller. Here, $z = 0$ shows the position of the boundary of the cylindrical vacuum chamber and a coaxial waveguide converter (i.d. $= 100$ mm and $L = 210$ mm). The chamber is evacuated by a rotary pump and 1500 1/s turbo molecular pump to a base pressure less than 1×10^{-7} Torr [working pressure is $P_{(Ar)} = (0.4–2.0) \times 10^{-3}$ Torr]. The magnetic mirror field is formed by the eight magnetic coils (64 mm width, 715 mm outer diameter). The frequency of the microwave is 2.45 GHz and the power P_μ can be delivered up to 1 kW. Microwaves are launched into a chamber as a circular TE_{11} mode into the vacuum chamber through the coaxial waveguide converter. The matching between the microwave circuit and the plasma is adjusted by a three-stub tuner and a movable metal plate in the coaxial waveguide to reduce the reflected microwave power detected by the power monitor as low as possible. By using this small diameter waveguide, the strong radial gradient in density is formed. The axial boundary condition is determined by metals on both ends of the vacuum chamber.

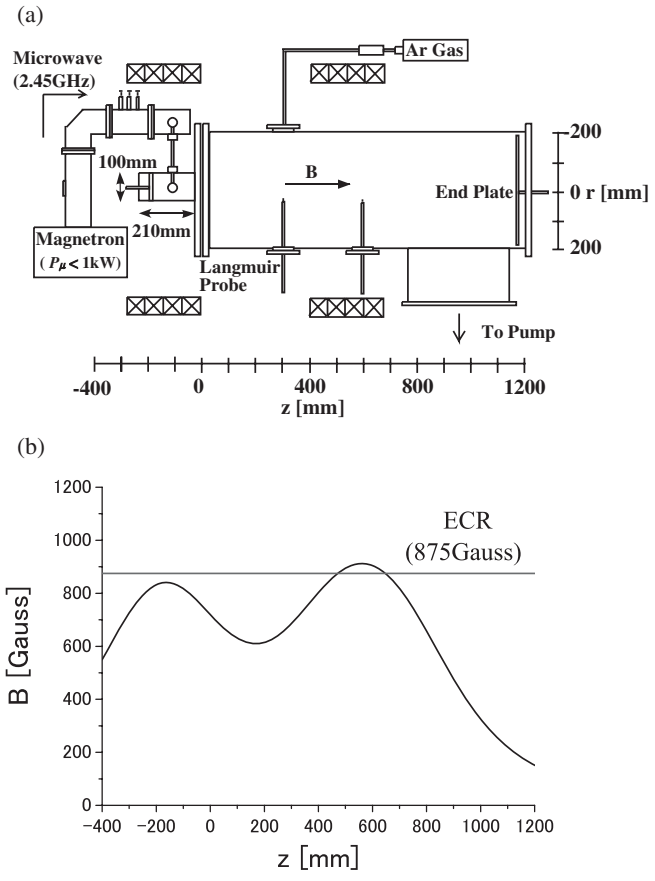

Fig. 1. (a) Schematic diagram of the experimental setup and (b) axial magnetic field profile.

The plasma parameters (electron density n_e, floating potential V_f and electron temperature T_e) and the plasma fluctuations are measured with Langmuir probes. The radial profiles of the mean plasma parameters are obtained from current–voltage (I–V) characteristics of the movable single Langumuir probe. Here, the single tungsten probe tip is 1 mm in diameter and 2 mm in length. Time evolution of ion saturation current I_{is} and V_f fluctuations is recorded by a data logger with a sampling rate of 1 MHz (16 bit). In addition, the Langumuir probes are set at eight azimuthal positions and five axial positions. The influence of these probes on the structure of plasma is negligibly small in this experiment. The azimuthal mode number m, parallel wave number n and azimuthal phase velocity can be deduced from these measurements. For measuring the phase shift between density fluctuations and potential fluctuations, a pair of axially separated ($\Delta z \sim 3$ mm) Langmuir probes is used. Both probes are located on fixed positions in the radial region with the strongest fluctuations (radius $r \sim 30$ mm).

Typical plasma parameters are: $n_e \sim 10^{17}\,m^{-3}$ and $T_e \sim 2$ eV (Table I: basic data are taken from refs. 30 and 31). The ionization rate is on the order of a few % (weakly ionized plasma). We note that not only the electron collisions but also the ion–neutral collisions are important for the stabilization of the collisional drift wave instability in

Table I. Typical plasma parameters.

Parameter	Typical value
Peak electron density (m^{-3})	2×10^{17}
Electron temperature (eV)	2
Ion temperature (eV) (assumption)	0.1
Filling gas pressure (Torr)	1×10^{-3}
Magnetic field strength (G)	685
Electron plasma frequency (Hz)	4.0×10^{9}
Ion plasma frequency (Hz)	1.5×10^{7}
Electron gyrofrequency (Hz)	1.7×10^{9}
Ion gyrofrequency (Hz)	2.3×10^{4}
Electron gyroradius (m)	5×10^{-5}
Ion gyroradius (m)	3×10^{-3}
Effective gyroradius (m) ($\rho_s = c_s/\omega_{ci}$)	1.3×10^{-4}
Electron–neutral collision frequency (Hz)	4.8×10^{5}
Electron–ion collision frequency (Hz)	1.1×10^{6}
Ion–neutral collision frequency (Hz)	1.6×10^{4}
Electron–neutral mfp (m)	1.2
Electron–ion mfp (m)	5.3×10^{-1}
Ion–neutral mfp (m)	3.2×10^{-2}
Here, $c_s = (k_B T_e/M)^{1/2}$, $\omega_{ci} = eB/M$	

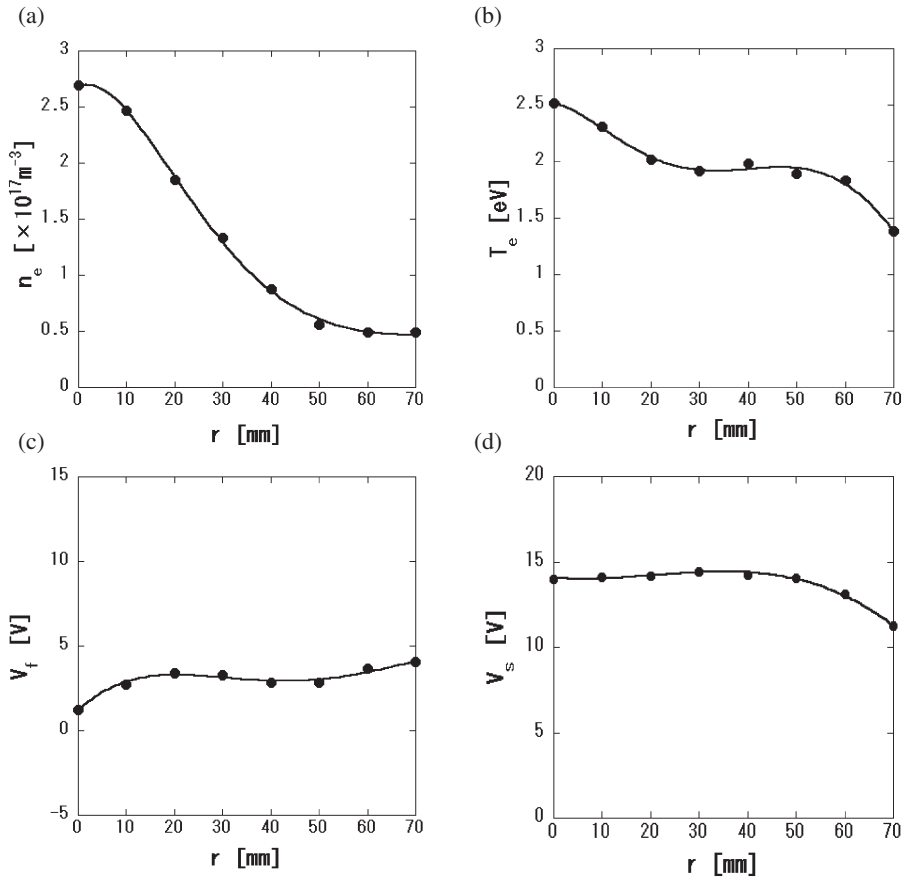

Fig. 2. Radial profiles of (a) electron density n_e, (b) electron temperature T_e, (c) floating potential V_f, and (d) space potential V_s.

this plasma because high neutral density shows that the ion–neutral particle mean free path (mfp) λ_{in} is smaller than the electron–neutral mfp λ_{en} and electron–ion mfp λ_{ei}.

3. Experimental Results

3.1 Profiles of plasma parameters

Figure 2 shows the radial profiles of n_e, T_e, V_f, and space potential V_s, which is calculated from the equation $V_s = V_f + \alpha T_e$ ($\alpha \cong 5.1$ for argon).[32] The radial density profile n_e (r) is peaked at $r = 0$ mm with a maximum value of 2.3×10^{17} m^{-3} and decreases steeply towards $r \sim 50$ mm. This relates to the radius of the coaxial waveguide of 50 mm.

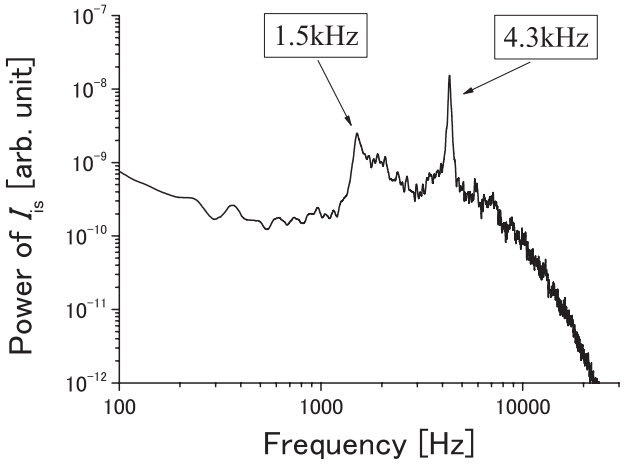

Fig. 3. Frequency spectrum of the ion saturation current.

The electron temperature profile T_e (r) is also peaked at $r = 0$ mm with a maximum value of ~2.5 eV and decreases weakly toward the plasma edge. The floating and space potential profiles, V_f (r) and V_s (r), remain relatively flat around ~3.5 and ~13 V, respectively. Since radial electric field E_r is <10 V/m and thus $\mathbf{E} \times \mathbf{B}$ drift velocity is $v_{\mathbf{E}\times\mathbf{B}} < 140$ m/s at $r \sim 20$–40 mm near the maximum density gradient region, this velocity is smaller than the electron diamagnetic drift velocity $v_{De} \sim 1000$ m/s at the same radial position, which is given by $v_{De} = (k_B T_e/eB) \times (1/n)(dn/dr)$. Here, $v_{\mathbf{E}\times\mathbf{B}}$ and v_{De} have the same direction. Throughout this paper, unless specified, the experimental conditions are as follows; the measurement point of $z = 300$ mm and $r = 27$ mm with $P_{(Ar)} = 1.0 \times 10^{-3}$ Torr, $P_\mu = 300$ W and the magnetic field strength $B = 685$ G.

3.2 Mode identification

A typical power spectrum of the ion saturation current is shown in Fig. 4. The two low frequency instabilities, whose frequencies are much smaller than the ion cyclotron frequency $f_{ci} \sim 26$ kHz, are observed in the ECR plasma. The frequency spectrum of I_{is} is characterized by the presence of two intense peaks with the frequencies f of ~1.5 and ~4.3 kHz. After this, we call the wave of $f \sim 1.5$ and 4.3 kHz, respectively, LFI (lower frequency instability) and HFI (higher frequency instability).

These observed two modes are identified as the drift wave and flute wave instabilities. Before showing this, we will present the general characteristics of the drift wave and flute wave instabilities.[33]

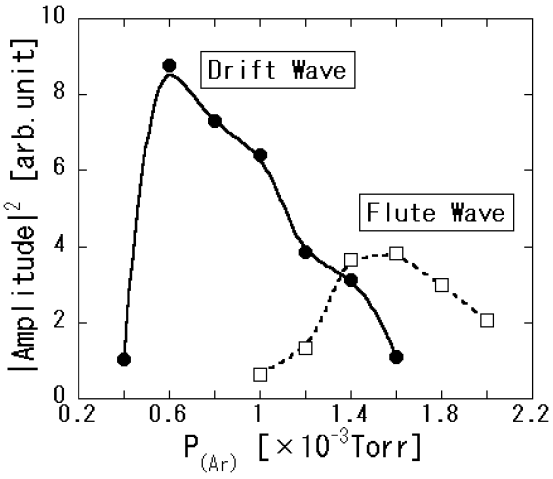

Fig. 4. Dependence of the square of fluctuation amplitude on the gas pressure.

Drift wave instability

(d-1) The drift wave instability is driven by a density gradient, (d-2) The fluctuation level $\tilde{n}/n_0$ peaks near the maximum radial density gradient and the normalized amplitudes of plasma density and potential fluctuations follow the relation of $\tilde{n}/n_0 \geq e\tilde{\phi}/k_B T_e$, (d-3) Density fluctuations lead the potential ones by phase difference $0 <$ phase $(\tilde{n}, \tilde{\phi}) < 45^\circ$, (d-4) The phase velocity in the azimuthal direction is given by v_{De} (the electron diamagnetic drift velocity) and most azimuthal unstable mode number is no restriction and (d-5) The parallel wave number is finite $k_\parallel \neq 0$ and is typically on the order of the inverse of the machine length.

Flute instability

(f-1) The flute wave instability is driven by the magnetic field gradient or curvature, (f-2) $\tilde{n}/n_0 \leq e\tilde{\phi}/k_B T_e$, (f-3) $40^\circ <$ phase $(\tilde{n}, \tilde{\phi}) < 90^\circ$, (f-4) The phase velocity in the azimuthal direction is given by $v_{E\times B}$ and most unstable azimuthal mode number is $m = 1$ or 2 and (f-5) $k_\parallel = 0$.

The characteristics of LFI and HFI are as follows (see Table II). In the both cases, the normalized amplitudes of $\tilde{n}/n_0$ and $e\tilde{\phi}/k_B T_e$ are relatively equal at the position of the maximum radial density gradient (for example, the both amplitudes in the region of LFI and HFI at 1.0×10^{-3} Torr are ~4 and ~10%, respectively). The density fluctuations lead the potential fluctuations by about 65–70° and about 40° in the region of LFI and HFI, respectively. At the location of high density fluctuations LFI and HFI propagate with the mode $m \approx 2$ and 4, respectively, in the direction of electron diamagnetic drift. The $\mathbf{E} \times \mathbf{B}$ drift propagates with $f_{E\times B} = (m/r)(v_{E\times B}/2\pi) < 1.5$–$3.0$ kHz ($m \approx 2$–4 at $r \approx 30$ mm) in the electron diamagnetic drift direction. LFI and HFI have different axial wave numbers $n \approx 0$ and 1 respectively. Here, $n = 1$ indicates that the half wavelength is the same as the device length. These results show that LFI and HFI are corresponding to the general characteristics of the flute wave and the collisional drift wave instabilities, respectively. It is noted that the observed frequency of HFI is significantly smaller than the drift frequency $\omega^*/2\pi = k_y v_{De}/(2\pi)$ with $k_y = m/r$, which is around 20 kHz at the location of the steepest density gradient. This will be explained by comparing the mode dispersion with Hasegawa–Wakatani model for actual discharge conditions in the next section.

Table II. Summary of features of LFI and HFI.

	LFI	HFI
Normalized amplitude	$\tilde{n}/n_0 \approx e\tilde{\phi}/k_B T_e$	$\tilde{n}/n_0 \approx e\tilde{\phi}/k_B T_e$
Phase delay of $e\tilde{\phi}/k_B T_e$ to $\tilde{n}/n_0$ (deg)	65–70	40
Azimuthal mode number m	2	4
Axial mode number n	0	1
Frequency (lab. frame) (kHz)	1.5	4.3
Doppler shill by $E \times B$ drift (kHz)	<1.5	<3

4. Comparison between Experimental and Numerical Results

4.1 Hasegawa–Wakatani model

Hasegawa–Wakatani model (with the effect of ion–neutral collision and equivalent gravitational acceleration g by the bad magnetic curvature) is utilized, in order to study the dependence of the growth rate of the collisional drift-interchange instability on the ion–neutral collision frequency. In this analysis, the local dispersion relation is evaluated. The magnetic field is specified to lie along the z axis, and the density gradient to be along the x axis. The azimuthal direction is the y axis. The equations governing the instability are vorticity eq. (1) and continuity eq. (2), which are given[34] as

$$\frac{\partial}{\partial t}\nabla_\perp^2 \phi = -\nu_{in}\nabla_\perp^2 \phi + C(\phi - n) - g\frac{\partial n}{\partial y}, \tag{1}$$

$$\frac{\partial}{\partial t} n + \kappa \frac{\partial \phi}{\partial y} = g\frac{\partial}{\partial y}(\phi - n) + C(\phi - n), \tag{2}$$

where $C = m_i k_\parallel / m_e \nu_e$, $\kappa = -\mathrm{d}n/\mathrm{d}r$, ϕ is the electrostatic potential, ν_{in} is the ion–neutral collision frequency, ν_e is sum of the electron–ion and electron–neutral collision frequencies ($\nu_e = \nu_{ei} + \nu_{en}$) and Ω_{ci} is the ion cyclotron angular frequency. In eqs. (1) and (2) the following normalization is used: $\Omega_{ci} t \to t$, $r/\rho_s \to r$, $n/n_0 \to n$, $e\phi/T_e \to \phi$. The local dispersion relation is given from eqs. (1) and (2) as

$$\omega = \frac{-\{\mathrm{i}[C(1 + k_\perp^2) + \nu_{in} k_\perp^2] - g k_\theta k_\perp^2\} \pm \sqrt{D}}{2k_\perp^2}, \tag{3}$$

$$\begin{aligned} D = {} & -C^2(1 + k_\perp^2)^2 - 2C\nu_{in}k_\perp^2(1 - k_\perp^2) - k_\perp^2 \nu_{in}^2 \\ & + k_\perp^2 k_\theta^2 g^2 (4 + k_\perp^2) - 4\kappa g k_\perp^2 k_\theta^2 \\ & + i\{4\kappa C k_\perp^2 k_\theta + 2k_\perp^2 k_\theta g[C(3 + k_\perp^2) - k_\perp^2 \nu_{in}]\}. \end{aligned}$$

In general, it describes the collisional drift-interchange mode, and contains the ideal interchange mode and the collisional drift mode as limiting cases. The dispersion relation for the interchange mode is recovered by taking the limit of $k_\parallel = 0$, (i.e., $C = 0$), $k_\perp \approx k_y$ and $\nu_{in} = 0$,

$$\omega = \frac{g k_y \pm \sqrt{g^2 k_y^2 - 4g\kappa}}{2} \Rightarrow \gamma \propto \sqrt{g\kappa}, \tag{4}$$

where γ represents the growth rate. The dispersion relation for the collisional drift mode is also obtained; Taking the limit of $g = 0$, $4k_\perp^2 k_y \kappa \ll C$ and $\nu_{in} = 0$, one has

$$\omega = \frac{-iC \pm \sqrt{4iCk_\perp^2 k_y\kappa - C^2}}{2k_\perp^2} \Rightarrow \gamma \propto \frac{k_y\kappa}{C} \propto \nu_e. \quad (5)$$

Equation (5) also illustrates that the real frequency of the collisional drift mode can be smaller than the drift frequency ω^*.

4.2 *Gas pressure (ion–neutral particle collision frequency) dependence*

We now study the coexistence of the collisional drift wave and flute mode. Figure 4 shows the square of the peak amplitude of the observed drift wave instability ($f \sim 4.3$ kHz) and that of the flute wave instability ($f \sim 1.5$ kHz) as a function of gas pressure. The drift wave is observed at a low filling pressure, $P_{(Ar)} = (0.4–1.6) \times 10^{-3}$ Torr. On the other hand, the flute wave is observed at a high filling pressure, $P_{(Ar)} = (1.0–2.0) \times 10^{-3}$ Torr. It is found that two modes coexist in a range of $P_{(Ar)} = (1.0–1.6) \times 10^{-3}$ Torr. The amplitude of the drift wave instability peaks at $P_{(Ar)} = 0.6 \times 10^{-3}$ Torr, then it decays and disappears in higher pressure regime, $P_{(Ar)} > 1.4 \times 10^{-3}$ Torr. The flute wave instability appears for $P_{(Ar)} > 1.0 \times 10^{-3}$ Torr, and the fluctuations are dominated by the flute mode in high filling pressure regime.

The coexistence of the collisional drift wave and flute mode is analyzed by considering the role of collisions of ions with neutral particles. The dependence of the growth rateγ, which is calculated using the Hasegawa–Wakatani model (choosing $g = 0.002$ and other parameters are taken from experimental observations), on the ion–neutral collision frequency ν_{in} is shown in Fig. 5(a). Here, ν_{in} is roughly proportional to $P_{(Ar)}$ in the low ionization degree, and the value ν_{in}/Ω_{ci} is estimated as $\sim$0.35 at $P_{(Ar)} \sim 0.6 \times 10^{-3}$ Torr in our experimental case (under the assumption of the constant ion temperature $T_i \sim 0.1$ eV and room temperature of neutral particle $T_n \sim 0.025$ eV). In this figure, $(m, n) = (4, 1)$ and $(m, n) = (2, 0)$ show the drift and flute modes, respectively. It is found that γ of $(4, 1)$ mode decreases as ν_{in}/Ω_{ci} increases. It is demonstrated that ν_{in} plays an important role in the stabilization of the drift wave instability. Then γ of $(2, 0)$ mode is larger than that of $(4, 1)$ mode in the region $\nu_{in}/\Omega_{ci} > 0.4$. From the comparison between Figs. 4 and 5(a), the coexistence of the $(4, 1)$ mode (drift wave instability) and the $(2, 0)$ mode (flute wave instability) is qualitatively understood.

Figure 5(b) shows the dependence of the various frequencies on the gas pressure. The experimental and numerical results of the collisional drift wave instability are plotted. For comparison, the drift wave frequency, shown as $\omega^*/2\pi = k_y v_{De}/2\pi$ is also plotted, which is obtained from the experimental values. As gas pressure increases, the drift wave frequency ω^* increases from $\sim$20 to $\sim$25 kHz and the observed frequency of the drift wave instability decreases from $\sim$5 to $\sim$3.5 kHz. As ν_{in}/Ω_{ci} increases, the calculated frequencies of the $(4, 1)$ mode decreases from $\sim$6.4 to $\sim$3.1 kHz, which is qualitatively in agreement with the result of the observed drift wave frequency. Here, the equilibrium $\mathbf{E} \times \mathbf{B}$ drift frequency is much smaller than ω^* and is not taken account in this calculation. It is found the observed and calculated mode frequencies are significantly smaller than the drift wave frequency ω^*. The comparison between

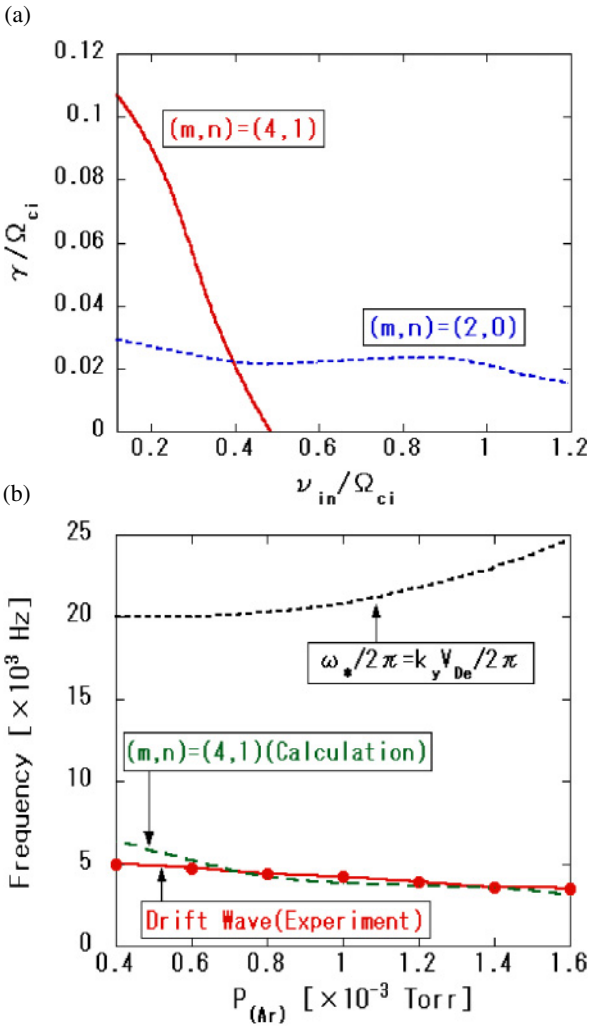

Fig. 5. (Color online) (a) Dependence of the growth rate on ion–neutral collision frequency obtained from the Hasegawa–Wakatani model and (b) Dependence of the various frequencies on the gas pressure.

the drift wave frequency ω^* and the real frequency of the collisional drift wave (given by the local dispersion relation) shows that real frequencies of the collisional modes strongly depend on the effects of collisions, ν_{in} and ν_e, whose effects are included in this model. On the other hand, it is found that the growth rate and frequency of the flute mode are weakly dependent on ν_{in} and ν_e, which is obtained from this model (not shown). In the above-mentioned experimental gas pressure region, the experimental and the numerical frequencies of the flute mode are almost constant.

5. Discussion and Conclusions

In this article, we reported the collisional drift wave instability and the flute wave instability in the linear ECR plasma device. It was found that, in addition to the flute wave instability, the drift wave mode can be destabilized by inducing steep density gradient [by the use of a coaxial waveguide-converter (i.d. = 100 mm)] and by imposing the axial boundary condition (the movable plate and the end plate). The basic features of plasma density and potential fluctuations showed that the observed fluctuations are identified as the collisional drift wave instability and the flute wave (interchange mode) instability, respectively. We

have found the experimental conditions where the drift wave and the flute wave instabilities coexist, only the drift wave is excited and vice verse: the amplitude of the collisional drift wave is high in the low-filling pressure regime and has the peak at $P_{(Ar)} \sim 0.6 \times 10^{-3}$ Torr; then it decrease above this. Above the high-pressure criterion, $P_{(Ar)} \sim 1.6 \times 10^{-3}$ Torr, the drift mode does not appear. In the intermediate regime, 1.0×10^{-3} Torr $< P_{(Ar)} < 1.6 \times 10^{-3}$ Torr, the drift mode and the flute mode are excited simultaneously. Moreover, the experimental range for the coexistence of two modes qualitatively agreed with the numerical analysis based on the Hasegawa–Wakatani model which describes the collisional drift-interchange mode with the effect of ν_{in}. The present result confirmed that ion–neutral particle collisions, which are proportional to the gas pressure, play an important role in the stabilization of the drift wave instability. In contrast, comparatively weak ion–neutral particle collisions are easy to excite the drift wave instability. The frequency of the observed collisional drift wave instability is smaller than the ω^* and is close to the numerical ones given by the local dispersion relation. It is found that the ν_{in} decreases the frequency of drift mode. The effect of ν_e is important for the destabilization mechanisms of the collisional drift wave. This model has demonstrated that the high ν_e leads to the decrease of the drift mode frequency. On the other hand, the growth rate and frequency of the flute mode are not affected much by ν_{in} and ν_e.

In this study, we have observed the both of the dissipative and the reactive instabilities controlling the neutral particle collision frequency. The plasma fluctuation is caused by the dissipative instability in the low ν_{in} regime, and the coexistence of the reactive and dissipative instabilities is realized in the intermediate range of the control parameters. This finding allows the experimental study of nonlinear interactions between the dissipative instability and reactive instability, which are also important for the anomalous transport in hot plasmas confined in toroidal devices. This interaction may explain some differences between the experiment result and the calculation one. The investigation of the nonlinear interaction between reactive mode and dissipative mode will be reported in future article.

Since the effect of the ion–neutral particle collisions play an important role for structure formation of the drift wave and flute wave instabilities, it is necessary to measure distributions of neutral particle density and ion temperature at each gas pressure in the experiment. In addition, the development of nonlinear and nonlocal simulation model is necessary for quantitative understanding of experimental results. These are left for the future work.

Acknowledgments

Authors wish to acknowledge fruitful discussion with Dr. A. Fujisawa and Dr. N. Kasuya. This work is partially supported by the Grant-in-Aid for Specially-promoted Research of Ministry of Education, Culture, Sports, Science and Technology (MEXT) of Japan (16002005) and by collaboration program of Research Institute for Applied Mechanics of Kyushu University. We also acknowledge the collaboration program of National Institute for Fusion Science, Japan.

1) P. H. Diamond, S.-I. Itoh, K. Itoh, and T. S. Hahm: Plasma Phys. Control. Fusion **47** (2005) R35.
2) W. Horton: Rev. Mod. Phys. **71** (1999) 735.
3) Y. Nagashima, K. Itoh, S.-I. Itoh, A. Fujisawa, K. Hoshino, Y. Takase, M. Yagi, A. Ejiri, K. Ida, K. Shinohara, K. Uehara, Y. Kusama, and the JFT-2M group: Phys. Rev. Lett. **95** (2005) 095002.
4) A. Hasegawa and K. Mima: Phys. Rev. Lett. **39** (1977) 205.
5) A. Hasegawa and M. Wakatani: Phys. Rev. Lett. **50** (1983) 682.
6) A. Hasegawa and M. Wakatani: Phys. Rev. Lett. **59** (1987) 1581.
7) H. Sugama, M. Wakatani, and A. Hasegawa: Phys. Fluids **31** (1988) 1601.
8) B. B. Kadomtsev and O. P. Pogutse: *Reviews of Plasma Physics* (Consultants Bureau, New York, 1970) Vol. 5, 249.
9) F. F. Chen: Phys. Rev. Lett. **15** (1965) 381.
10) H. W. Hendel, B. Coppi, F. Perkins, and P. A. Politzer: Phys. Rev. Lett. **18** (1967) 439.
11) P. A. Politzer: Phys. Fluids **14** (1971) 2410.
12) T. Klinger, A. Latten, A. Piel, T. Pierre, G. Bonhomme, and T. Dudock de Wit: Phys. Rev. Lett. **79** (1997) 3913.
13) M. Kono and M. Tanaka: Phys. Rev. Lett. **84** (2000) 4369.
14) C. Schröder, T. Klinger, D. Block, A. Piel, G. Bonhomme, and V. Naulin: Phys. Rev. Lett. **86** (2001) 5711.
15) M. Light, F. F. Chen, and P. L. Colestock: Phys. Plasmas **8** (2001) 4675.
16) T. Kaneko, H. Tsunoyama, and R. Hatakeyama: Phys. Rev. Lett. **90** (2003) 125001.
17) C. Schröder: Ph. D. Thesis, Ernst-Moritz-Arndt University, Greifswald (2003).
18) C. Schröder, O. Grulke, T. Klinger, and V. Naulin: Phys. Plasmas **11** (2004) 4249.
19) E. Gravier, F. Brochard, G. Bonhomme, T. Pierre, and J. L. Briancon: Phys. Plasmas **11** (2004) 529.
20) V. Sokolov and A. K. Sen: Phys. Rev. Lett. **92** (2004) 165002.
21) F. Brochard, E. Gravier, and G. Bonhomme: Phys. Plasmas **12** (2005) 062104.
22) M. J. Burin, G. R. Tynan, G. Y. Antar, N. A. Crocker, and C. Holland: Phys. Plasmas **12** (2005) 052320.
23) F. Brochard, G. Bonhomme, E. Gravier, S. Oldenbürger, and M. Philipp: Phys. Plasmas **13** (2006) 052509.
24) G. R. Tynan, C. Holland, J. H. Yu, A. James, D. Nishijima, M. Shimada, and N. Taheri: Plasma Phys. Control. Fusion **48** (2006) S51.
25) S. Shinohara, T. Nishijima, M. Kawaguchi, K. Terasaka, Y. Nagashima, T. Yamada, T. Maruta, Y. Kawai, M. Yagi, S.-I. Itoh, A. Fujisawa, and K. Itoh: Proc. 48th Annu. Meet. Division of Plasma Physics, Philadelphia, 2006, Vol. 51, p. 162.
26) N. Kasuya, M. Yagi, and K. Itoh: J. Plasma Phys. **72** (2006) 957.
27) M. Koga and Y. Kawai: Phys. Plasmas **10** (2003) 650.
28) H. Tsuchiya, K. Kamataki, M. Koga, M. Fukao, S. Shinohara, and Y. Kawai: Proc. 27th ICPIG, 2005, No. 14-201.
29) K. Kamataki, Y. Nagashima, S. Shinohara, Y. Kawai, M. Yagi, K. Itoh, and S.-I. Itoh: Proc. 33rd EPS Conf. Plasma Physics, Roma, 2006, P2.045.
30) S. C. Brown: *Basic Data of Plasma Physics, 1966* (M.I.T. Press, Cambridge, MA, 1967) 2nd ed., p. 22.
31) M. A. Lieberman and A. J. Lichtenberg: *Principles of Plasma Discharges and Material Processing* (Wiley, New York, 1994) p. 80.
32) I. H. Hutchinson: *Principle of Plasma Diagnostics* (Cambridge University Press, Cambridge, 2002) 2nd ed., p. 55.
33) D. L. Jassby: Phys. Fluids **15** (1972) 1590.
34) M. Yagi: Ph. D. Thesis, Kyoto University, Kyoto (1989).